

1       **Engineering a superwetting thin film nanofibrous composite membrane**  
2               **with excellent antifouling and self-cleaning properties to separate**  
3                       **surfactant-stabilized oil-in-water emulsions**

4  
5  
6                               Miao Tian<sup>1</sup>, Yuan Liao<sup>1,3</sup>, Rong Wang<sup>1,2\*</sup>

7  
8                               1. Singapore Membrane Technology Centre,  
9       Nanyang Environment and Water Research Institute, Nanyang Technological University, 1  
10                               Cleantech Loop, Singapore 637141, Singapore

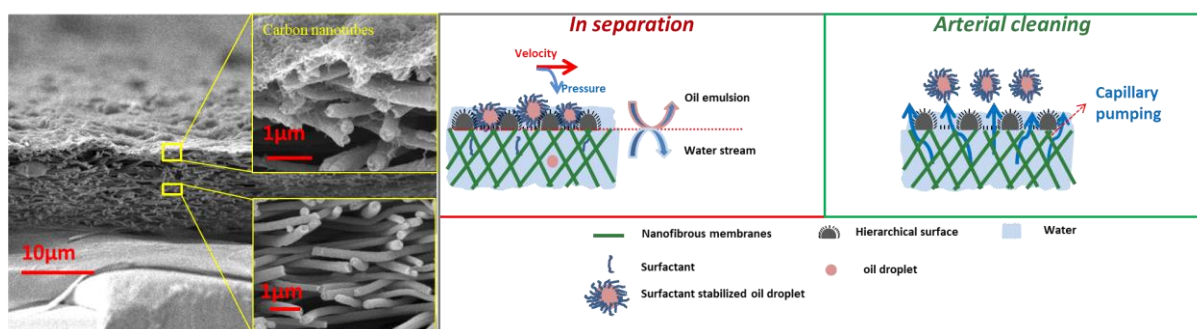
11  
12                               2. School of Civil and Environmental Engineering, Nanyang Technological University,  
13                               50 Nanyang Avenue, Singapore 639798, Singapore

14  
15                               3. Sino-Canada Joint R&D Centre for Water and Environmental Safety, College of  
16                               Environmental Science and Engineering, Nankai University, Tianjin 300071, China

17  
18  
19  
20  
21                               \*Corresponding author at: School of Civil and Environmental Engineering,  
22                               Nanyang Technological University, 639798 Singapore,  
23                               Singapore. Tel.: +65 6790 5327; fax: +65 6791 0676.  
24                               E-mail address: rwang@ntu.edu.sg (R. Wang).

26 **Abstract**

27 In recent years, novel superwetting membranes have gained popularity for oily wastewater  
28 treatments via synergy between surface chemistry and topography. However, the water fluxes  
29 of the superwetting membranes normally decrease rapidly due to pore clogging and surface  
30 fouling, especially when treating surfactant-stabilized oil-in-water emulsions. Herein, a facile  
31 strategy is proposed to develop a superwetting thin film nanofibrous composite (TFNC)  
32 membrane with remarkable antifouling and self-cleaning properties to effectively separate  
33 surfactant-stabilized oil-in-water emulsions. The membrane is composed of an ultrathin carbon  
34 nanotubes (CNTs)-polyvinyl alcohol (PVA) composite skin layer, and a highly porous  
35 electrospun nanofibrous substrate as well as a non-woven mechanical support. The robust  
36 three-dimensional (3D) CNTs composite skin layer were immobilized on the nanofibrous  
37 substrate surface by crosslinking the CNTs with PVA. This skin layer serves as a functional  
38 barrier to reject oil droplets, which exhibited excellent performance in treating surfactant-  
39 stabilized oil-in-water emulsions with a rejection of 95% and a competitive flux of  $\sim 60 \text{ Lm}^{-2}\text{h}^{-1}$   
40 under an ultra-low pressure (20 kPa) in a cross-flow filtration process. Moreover, the CNTs  
41 composite layer also protects the membrane surface from fouling. The TFNC membrane  
42 possesses outstanding reusability, as the water flux could be recovered by 100% in a continuous  
43 cyclic operation without cleaning, which should be attributed to the underwater oil repellence  
44 of its superhydrophilic surface and self-cleaning property based on the capillary pumping effect  
45 occurred in the micron/nano-channels of the membrane surface.



46

47 **Keywords:** surfactant-stabilized oil-in-water emulsion; thin film nanofibrous composite  
48 membrane; superwetting; carbon nanotubes; self-cleaning  
49

## 50 **1 Introduction**

51 Extensive activities in petrochemical, metallurgical, food and pharmaceutical industries have  
52 produced increasing amounts of oily wastewater around the world[1, 2]. Due to their adverse  
53 impacts on both ecosystem and human health, it is highly desirable yet challenging to treat the  
54 oily wastewater using efficient, energy- and cost-effective technologies[1, 3, 4]. The oil/water  
55 mixtures may present in multiple forms: oil/water layered solutions (droplet size greater than  
56 150  $\mu\text{m}$ ), surfactant-free (droplet size between 20-150  $\mu\text{m}$ ) and surfactant-stabilized (droplet  
57 size less than 20  $\mu\text{m}$ ) oil-in-water and water-in-oil emulsions[5]. The unstable oil/water layered  
58 solutions or surfactant-free oil/water emulsions can be readily treated by conventional  
59 separation technologies, such as gravity separation, flotation and skimming[6]. The most  
60 challenging issue is to separate surfactant-stabilized oil-in-water emulsions which have the oil  
61 droplets size down to one micron and are stably dispersed in water by surfactants. A long  
62 residence time and even chemical addition are required to enable the conventional separation  
63 techniques to be effective. This calls for new promising methods.

64

65 To handle surfactant-stabilized oil-in-water emulsions, membrane technology offers an  
66 alternative solution because of its acceptable permeate quality, low capital costs, small  
67 footprints, absent chemical additions and simple operations[7, 8]. However, in spite of these  
68 advantages, the pressurized membrane filtration such as ultrafiltration (UF) and nanofiltration  
69 (NF) often encounter serious membrane fouling due to surfactant adsorption and pore clogging  
70 by oil droplets, which resulted in a significant reduction in membrane permeability and  
71 rejection[9, 10]. To make it worse, the high operating pressure up to several bars required in  
72 UF and NF processes not only accelerates the membrane fouling but also increases energy  
73 consumption. Additionally, these UF and NF membranes showed poor recoverability after  
74 cleaning [10, 11].

75 Various novel membranes with special wettability have been extensively developed for  
76 oil/water separation[12-16]. Inspired by fish scales, the superhydrophilic and underwater  
77 superoleophobic surfaces which shows an in-air water contact angle of  $0^\circ$  and underwater oil  
78 contact angle higher than  $150^\circ$  have been fabricated to remove water from oil-in-water  
79 mixtures[6, 17-19]. The superhydrophilic materials have water-favourite properties and tend  
80 to trap abundant water on their rough surfaces. As water usually exhibits a higher density than  
81 oils, the trapped water can serve as a barrier on materials surface to reject oil droplets and  
82 greatly reduce the direct contact area between oils and materials, which results in low oil-  
83 adhesion and mitigates the fouling propensity. In our previous work, a novel membrane with  
84 switchable superwettability for oil and water was developed by electrospinning and surface  
85 modification [20, 21]. The membrane can treat various types of oil/water mixtures, including  
86 simple layered solutions and emulsions without external driving force or under an ultra-low  
87 pressure. However, it displayed a rapid decline of water flux when separating surfactant-  
88 stabilized oil-in-water emulsions. Further studies to alleviate membrane fouling and enhance  
89 the self-cleaning property of the membrane when treating the surfactant-stabilized oil-in-water  
90 emulsions are of great significance.

91

92 A number of surface modification approaches, such as self-assembly, chemical etching, atom  
93 transfer radical polymerization (ATRP) and chemical vapour deposition (CVD), have been  
94 adopted to fabricate the anti-fouling and self-cleaning surfaces[22, 23]. However, these  
95 modified membranes required tedious modification steps, special facilities and costly  
96 chemicals[13, 24]. Electrospinning is a versatile method to generate continuous nanofibers with  
97 a 3D network architecture[19, 25]. The nanofibrous surface with micro-scale roughness could  
98 be altered to become hierarchically micro/nano-scaled by further surface modification[26].  
99 Although electrospun membranes have shown promising performance for oil/water separation,

100 the anti-fouling properties of these membranes require improvement when dealing with  
101 surfactant-stabilized oil-in-water emulsions. Formation of a thin film layer on the membrane  
102 surface can reduce the opening area between the overlapping point of nanofibers, prevent the  
103 intrusion of foulants and enhance surface hydrophilicity, which is expected to enhance  
104 antifouling and self-cleaning properties [24, 27].

105

106 Recent advances in nanotechnology have expanded the application of nano-materials to  
107 membrane technologies. Carbon nanotubes (CNTs) have attracted tremendous interests in  
108 membrane development, attributed to its three-dimensional (3D) network structure,  
109 outstanding mechanical, thermal, porous and tubular structures [8, 26, 28-31]. Theoretically,  
110 functionalized CNTs can increase membrane hydrophilicity and provide better fouling  
111 resistance. Recently, the CNTs have been incorporated into a polymer matrix to develop hybrid  
112 foams for oil/water separation[32]. However, the incorporation of CNTs in a polymeric matrix  
113 requires a large amount of expensive materials (normally 5~10 wt. %), which may hinder their  
114 large-scale manufacture[8, 33]. Moreover, most CNTs are easily wrapped or embedded in the  
115 thick polymer matrix and their superior intrinsic properties cannot be fully utilized[34].

116

117 By taking the advantages of electrospun nanofibrous membranes and CNTs, we report a low-  
118 cost and mass-producible approach to fabricate a thin film nanofibrous composite (TFNC)  
119 membrane with excellent antifouling and self-cleaning properties, which is specially designed  
120 for separating surfactant-stabilized oil-in-water emulsions. The self-cleaning is expected to be  
121 achieved via the capillary pumping effect, a nano-scale fluid transport phenomenon in  
122 hierarchical nano-channels without the supply of external energy, which has found vast  
123 applications spanning from water desalination to biotechnology[35-37]. A tri-layer TFNC  
124 membrane was prepared by spraying an ultra-thin CNTs selective layer on the top of

125 electrospun polyacrylonitrile (PAN) nanofibrous intermediate layer, which was supported by  
126 non-woven mechanical support. The CNTs skin layer was cross-linked by poly (vinyl alcohol)  
127 (PVA). The as-prepared membrane was characterized comprehensively and batch filtration  
128 studies were performed to examine the influence of oil types, applied hydraulic pressure on the  
129 water permeability and oil removal efficiency. Moreover, the fouling resistance and self-  
130 cleaning property of the membrane were evaluated in a 4-hour continuous crossflow operation.

131

## 132 **2 Experimental**

### 133 2.1 Membrane materials and chemicals

134 Unless otherwise specified, all chemicals were used as received without further purification.  
135 COOH functionalized Multi-walled carbon nanotubes (8-15 nm in diameter, purity of >95 wt%,  
136 with a functional group content of 2.5 %) were purchased from Cheaptubes, USA.  
137 Poly(ethylene terephthalate) (PET, Grade 3233, Ahlstrom, USA) nonwoven mesh was used as  
138 mechanical support. Commercial polyacrylonitrile (PAN, Mw 150,000) purchased from  
139 Sigma-Aldrich, Singapore was used to fabricate nanofibrous substrates. N, N-  
140 dimethylformamide (DMF, >99.5%) and Isopropyl alcohol (IPA) with analytical grade were  
141 provided by Merck, Singapore. Polyvinyl alcohol (PVA, Mw 12,000 to 14,000, 87-88%  
142 hydrolyzed) was purchased from Sinopharm Chemical Reagent Co., Ltd. The Polybead® with  
143 a diameter of 100 nm (Cat#16688) was purchased from Polysciences, Inc. to characterize the  
144 membrane pore size in crossflow filtration. Petroleum with 18% aromatics basis purchased  
145 from Sigma-Aldrich (Singapore) was used to represent industrial oils. Canola oil (100% pure  
146 canola oil) was purchased from the supermarket to represent food oils. Tween® 20 was used  
147 as a surfactant to prepare oil-in-water emulsions. Ultrapure water (DI water) with a resistivity  
148 of 18.2 MΩ.cm (Millipore Integral 10 Water Purification System) was used to prepare all the

149 aqueous solutions. A PVDF commercial membrane purchased from GE Osmonics (SKU.  
150 PV2HY320F5) was used as a reference.

151

## 152 2.2 Electrospinning of nanofibrous substrate

153 To prepare a PAN dope solution, PAN polymer powder with the desired amount was dissolved  
154 in DMF by stirring at 80 °C. The 8 wt% PAN solution was firstly fed to a spinneret (inner  
155 diameter (ID) = 0.75 mm, outer diameter (OD) = 1.59 mm) at a controlled flow rate by a syringe  
156 pump and then electrospun to nanofibers on PET non-woven support using an electrospinning  
157 apparatus (MJESPIN-08-01, SBTG, Inc, USA) described in our previous work[38, 39]. A thin  
158 PAN nanofibrous layer with a thinner nanofiber diameter was then electrospun on the surface  
159 of the coarse PAN nanofiber surface by electrospinning the 5 wt% PAN dope which was kept  
160 in a fume hood overnight to remove the residual solvent. After that, the nanofibrous support  
161 was heat-pressed at 100 °C for 1 h to enhance the integrity of the nanofibrous substrate, which  
162 was labelled as PAN. [The heat-pressed temperature is selected following the principle that a  
163 bit higher than the glass transition temperature \(~96 °C\) and much lower than the fusion  
164 temperature \(~322 °C\) of the material PAN in order to preserve fiber structure.](#) The detailed  
165 electrospun parameters of the nanofibrous substrates are summarized in **Table 1**.

166 **Table 1** Electrospun conditions for preparation of the nanofiber supports.

Sample code	PAN	
	Top	Bottom
Polymer dope	5% PAN	8% PAN
Flow rate ( $\mu\text{L}/\text{min}$ )	15	15
Applied voltage (kV)	20	20
Working distance (cm)	12	12
Humidity	40 $\pm$ 2 %	40 $\pm$ 2 %

167

168

### 169 2.3 Membrane modification

170 An ultrathin CNTs barrier layer was formed on the aforesaid PAN nanofibrous substrate via  
171 spray coating. In brief, we used water as the wetting liquid to occupy the pores in the nanofiber  
172 substrates as the membrane is superhydrophilic. A rubber roller was used to remove excessive  
173 water on the substrate surfaces. On the top of the wetted PAN nanofibrous support layer, a thin  
174 CNTs layer was prepared by spraying a well-mixed CNTs/PVA solution (0.2 wt% CNTs and  
175 0.05 wt% PVA) and 0.05 wt% Glutaraldehyde (GA) solution using a customized spray-coating  
176 machine (7000 Dispenser Robot, Spraying Systems Co. (s) PTD LTD)[40]. The pressure in  
177 spray coating system was adjusted as well in order not to let the selective layer penetrating into  
178 pores. The membrane was then cured at 60 °C for 20 min to cross-link and stabilize the CNTs  
179 on the membrane surface. The CNTs amount deposited on the membrane surface was 1 g/m<sup>2</sup>  
180 (~2 wt %). The pressure of the coating process should be adjusted in the range of 0.2~1 bar  
181 based on a different substrate. The pre-wetting agent may need to prevent penetration of the  
182 coating layer into the substrate. The resulted membrane was washed with DI water and stored  
183 in water prior to further testing and characterization. The membrane coated with a CNTs barrier  
184 layer was coded as CNTs-PAN.

185

### 186 2.4 Characterization of as-prepared composite membranes

187 Membrane thickness was measured using a micrometer ( $\pm 4.06 \mu\text{m}$  accuracy)[41]. The pore  
188 size and pore size distribution of the membrane substrate were analysed using a capillary flow  
189 porometer (CFP 1500A, Porous Materials, Inc, USA). The membrane's mechanical properties  
190 were characterized using a Zwick Universal Testing Machine, USA. The in-air water and  
191 underwater oil contact angles of as-fabricated membranes were measured using a goniometer

192 (Contact Angle System OCA, Data Physics Instruments GmbH, Singapore). The surface and  
193 cross-sectional morphologies of the PAN and CNTs-PAN were characterized using a field  
194 emission scanning electron microscopy (FESEM, JSM7200F, JEOL Asia Pte Ltd, Japan). The  
195 samples were coated with platinum using a sputter coater (JEOL JFC-1600) at 20 mA for 40 s.  
196 The surface topography of individual nanofibers was characterized using an XE 100 atomic  
197 force microscopy (AFM, Park Systems, Korea). For each sample, an area of  $5.0\ \mu\text{m} \times 5.0\ \mu\text{m}$   
198 was scanned using non-tapping mode. At least three samples of nanofibers were analysed to  
199 obtain the average root mean square roughness. Nanofiber diameter was analysed using  
200 software *FoxitPDF Reader*. About 100 nanofibers were measured to get the average value and  
201 standard deviation.

202

## 203 2.5 Preparation and characterization of oil-in-water emulsions and separation tests

204 Oil concentration in wastewater generated in the industries mentioned in the introduction  
205 section ranges from 50 to 1000 mg/L. Thus, we used 1000 mg/L to simulate the worst situation.  
206 The surfactant-stabilized oil-in-water emulsions were prepared using a laboratory blender  
207 (Waring Lab Blender). Briefly, 1000 mg of oil and 100 mg of Tween® 20 were added into 1  
208 L DI water, which was blended with a speed of 18000 rpm for 1 min. The weight ratio between  
209 oil and surfactant was kept at 10:1. The droplet sizes were measured by a Mastersizer (Malvern  
210 Hydro 2000SM). The Total Organic Carbon (TOC) of oil-in-water emulsions and permeates  
211 were analysed by Shimadzu TOC Analyzer (Model: TOC-v CSH).

212

213 Oil/water separation performance was measured by a cross-flow filtration setup elsewhere. In  
214 brief, a membrane coupon with an effective membrane area of  $28\ \text{cm}^2$  was compacted using DI  
215 water at an applied pressure of 20 kPa for 1 h prior to the water flux measurement. The flow  
216 channel dimension of the cell is  $1 \times 29 \times 75\ \text{mm}$ . Diamond-patterned spacers were placed in both

217 the feed and permeate fluid channels. The prepared surfactant-stabilized oil-in-water emulsions  
218 were pumped by a variable-speed peristaltic pump through the membrane cell at a hydraulic  
219 pressure of 20-100 kPa (0.2-1.0 bar) with a velocity of 18 cm/s. Water permeated through the  
220 membrane was collected in a beaker and weighted on an electrical balance to calculate  
221 membrane flux. The water flux was measured by monitoring the weight change of the permeate.  
222 The rejection (R) was calculated according to the TOC difference between the feed and  
223 permeate water.

$$224 \quad R = \left(1 - \frac{C_p}{C_f}\right) \times 100\%$$

225 where  $C_f$  and  $C_p$  represent the TOC of the feed and permeate water, respectively.

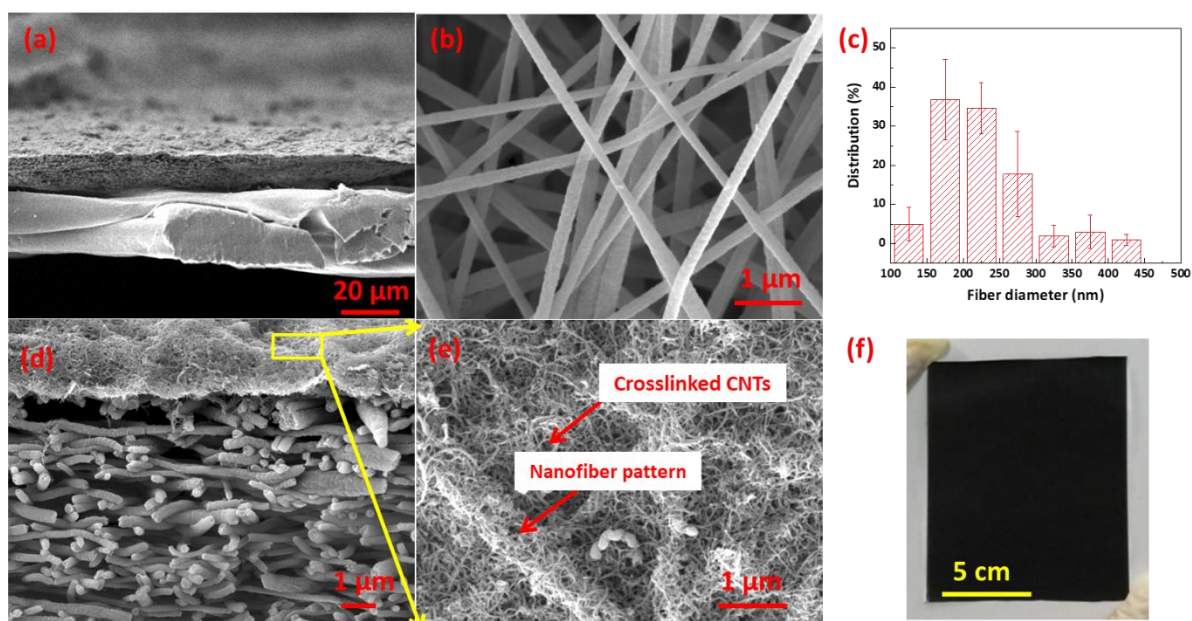
226 In the cyclic study of membrane fouling, the cross-flow filtration was stopped to rest the CNTs-  
227 PAN membrane for 20 minutes. Then a new cycle test with the same feed solution was started.

228

### 229 **3 Results and Discussion**

#### 230 **3.1 Membrane structure**

231 The CNTs-PAN membrane with a thickness of 54  $\mu\text{m}$  is composed of a nonwoven support  
232 layer, a PAN nanofibrous layer and a crosslinked CNTs layer (**Figure 1a**). The PAN  
233 nanofibrous substrate has an open and interconnected porous structure (**Figure 1b**). The  
234 average PAN nanofiber diameter is  $\sim 200$  nm (**Figure 1c**). An ultrathin crosslinked CNTs layer  
235 with a thickness around 200 nm was formed on the top of the substrate through a spray coating  
236 system (**Figure 1d**). The FESEM surface morphology of CNTs-PAN (**Figure 1e**) and the  
237 image shown in **Figure 1f** confirms that the carbon nanotubes are connected with each other  
238 to form a uniform and ultrathin film to fully cover the PAN nanofibrous membrane.



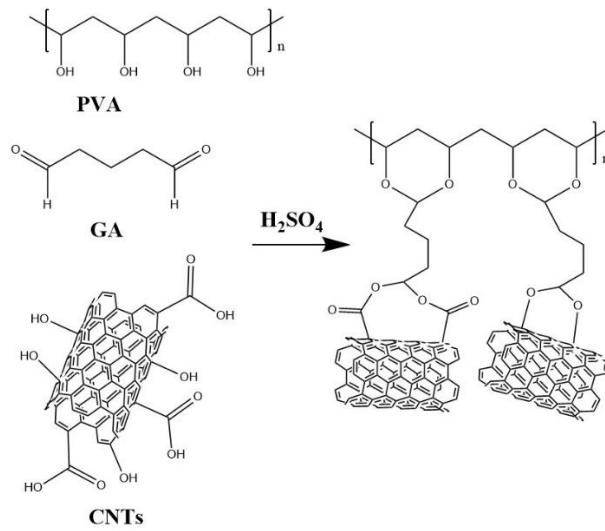
239

240 **Figure 1** FESEM images of (a) cross-sectional CNTs-PAN nanofibrous membrane, (b)  
 241 surface of PAN nanofibrous membrane, (c) nanofiber diameter distribution of the PAN  
 242 nanofibrous membrane, (d) cross-sectional FESEM image of the ultrathin crosslinked CNTs  
 243 coated PAN nanofibrous membrane (CNTs-PAN), (e) surface image of the CNTs-PAN  
 244 membrane. (f) photograph of CNTs-PAN membrane (membrane size 12×12 cm).

### 245 3.2 CNTs and PVA crosslinking

246 The COOH group and OH group of CNTs can be linked with -OH group of PVA via  
 247 Glutaraldehyde with the acid catalyst at 60 °C[31, 42]. A schematic illustration of the  
 248 crosslinking mechanism is shown in **Figure 2**. XPS narrow scan spectra of CNTs (**Figure 3 a**  
 249 **& b**) and CNTs-PAN membrane (**Figure 3 c & d**) further reveals that C=O /C-O ratio reduced  
 250 in CNTs-PAN after crosslinking. The reduction of chemical bond C=O is associated with the  
 251 cross-linking of GA with carboxylic groups present on CNT-COOH, indicating the GA is  
 252 forming ester bonds with the CNT-COOH. The crosslinking of the CNT-COOH and PVA  
 253 preventing the CNTs from desorbing and entering the retentate or permeate streams. XPS  
 254 characterization shows that a decreasing amount of C=O bonds in CNTs-PAN, which confirms  
 255 the chemical cross-linking between -COOH groups of CNTs and PVA via glutaraldehyde.  
 256 Moreover, a CNTs selective layer with a coating density of 1g/m<sup>2</sup> was developed in this work  
 257 by tuning the coating time and dope composition, which is promising for large-scale production.

258

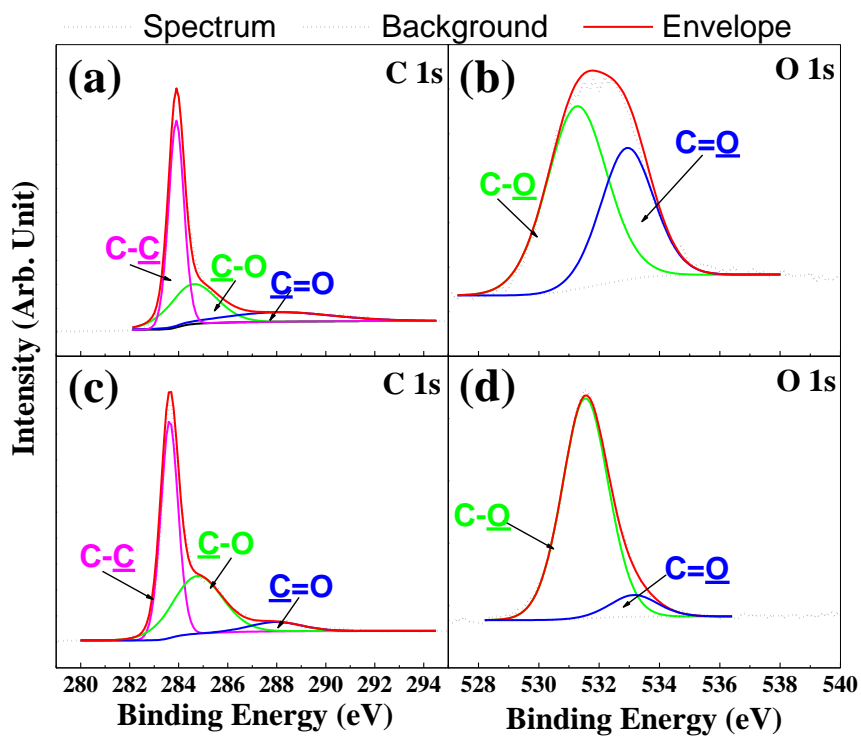


259

260

**Figure 2** A schematic illustration of the crosslinking mechanism.

261



262

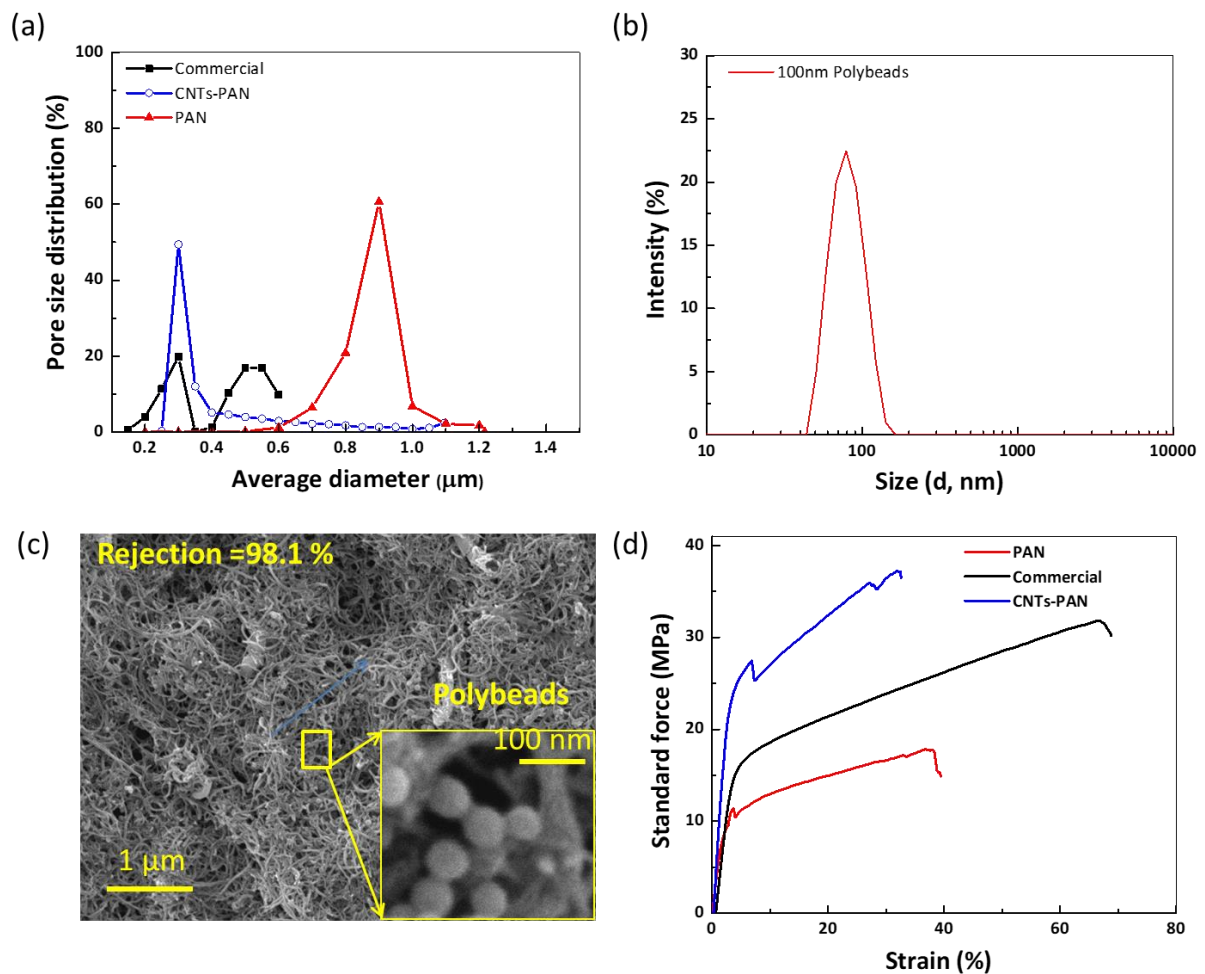
263 **Figure 3** XPS narrow scan spectra of CNTs for elements C 1s (a) and O1s (b);

264 CNTs-PAN membrane for elements C 1s (c) and O 1s (d)

265

266 3.3 Membrane intrinsic property

267 The pore size distributions characterized by the capillary flow porometer of the three  
 268 membranes are presented in **Figure 4 a**. It can be seen that the CNTs-PAN has a narrow pore  
 269 size distribution with a mean pore size around 250 nm, which is more uniform and smaller than  
 270 the PAN support and the commercial membrane. To evaluate the membrane's rejection towards  
 271 small particles during the cross-flow filtration, commercial uniform polybeads® with particle  
 272 size of 100 nm was utilized to characterize the membrane pore size. The particle size  
 273 distribution demonstrates that the average size of the polybeads is  $77\pm 0.4$  nm (**Figure 4 b**).  
 274 The CNTs-PAN shows a rejection of 98% to these small rigid polymer beads (**Figure 4 c**). The  
 275 membrane mechanical strength test also shows that the ultrathin CNTs layer enhances the  
 276 membrane tensile modulus by 20%, which should be attributed to the super mechanical  
 277 strength of CNTs and PVA cross-linking (**Figure 4 d**).



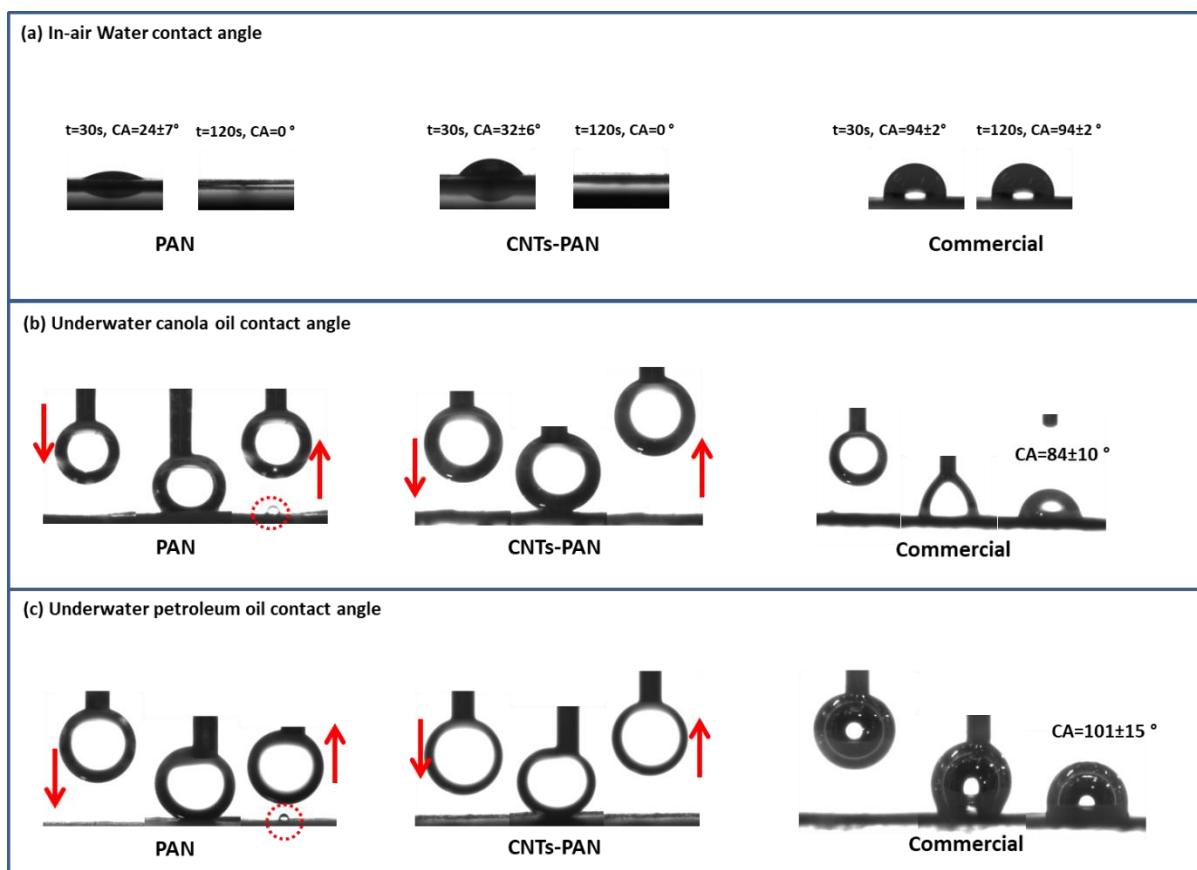
278

279 **Figure 4** (a) Pore size distribution of the three membranes; (b) 100 nm Polybead® size  
280 distribution characterized by zetasizer; (c) FESEM image of the CNTs-PAN membrane after  
281 filtration of Polybead®; (d) a group of representing mechanical force vs strain curves of three  
282 membranes.

### 283 3.4 Surface wetting properties

284 In-air water contact angles and underwater oil contact angles were used to characterize the  
285 surface wettability of as-prepared membranes and the commercial membrane. As shown in  
286 **Figure 5 (a)**, after dropping a 5 $\mu$ L water droplet on the membrane surface for 30 seconds, the  
287 water contact angles of PAN, CNTs-PAN and the commercial membrane are  $24 \pm 7^\circ$ ,  $32 \pm 6^\circ$   
288 and  $94 \pm 2^\circ$ , respectively. After 120 seconds, the water contact angles of PAN and CNTs-PAN  
289 membranes are  $0^\circ$  due to their superhydrophilicity and highly porous structure. These surface  
290 properties should be attributed to the polar nitrile group in PAN and unreacted  
291 hydroxyl/carboxyl groups of PVA crosslinked CNTs[43, 44]. **Figures 5(b)** and **5(c)** show the  
292 underwater canola oil and petroleum contact angles of the three membranes. Both PAN and  
293 CNTs-PAN membranes showed an underwater superhydrophobicity towards canola oil and  
294 petroleum. After cycles of compression, the oil droplet could be eventually broken and a small  
295 droplet (marked in the dotted circle) was observed to attach on the micro-structured PAN  
296 membrane due to the deformation of the oil droplet under pressure and relatively flat surface  
297 microstructure. In contrast, the oil droplet cannot readily attach onto the CNTs-PAN membrane  
298 surface even under cycles of physical compression, which should be attributed to its robust  
299 hierarchically multi-structured surface shown in **Figure 1(e)**. The surface leads to the lowest  
300 contact area of applied oil droplet and thus reduces oil adhesive force significantly. Compared  
301 to the PAN and CNTs-PAN membranes, the commercial membrane with flat surface shows  
302 lower underwater oil contact angles of  $84 \pm 10^\circ$  and  $101 \pm 15^\circ$  towards canola oil and petroleum,  
303 respectively. A demonstrated video (video 1) is presented in the support information (SI) for a  
304 better view of the underwater superoleophobicity.

305



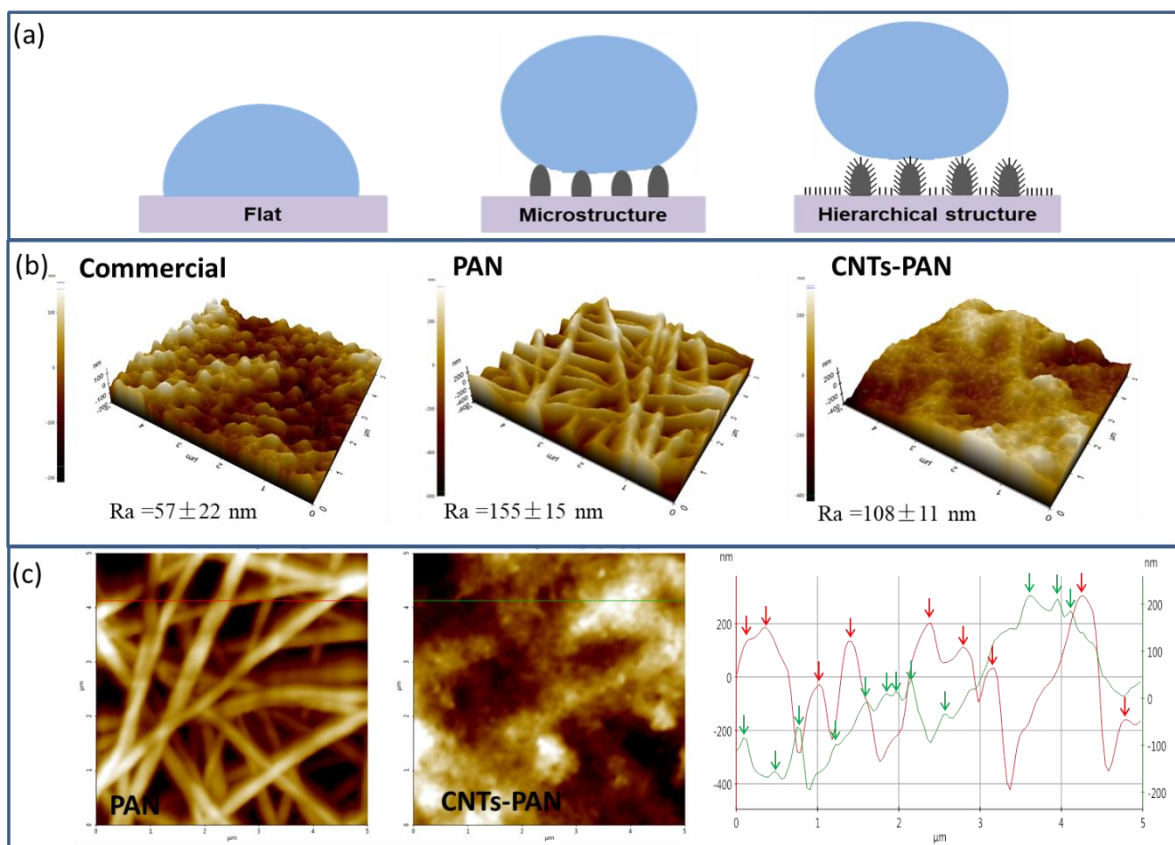
306

307 **Figure 5** (a) Static water contact angle (WCA), (b) underwater dynamical wetting behaviour  
 308 of canola oil, (c) underwater dynamical wetting behaviour of petroleum of PAN, CNTs-PAN,  
 309 and a commercial membrane. The small oil droplets are marked in the dotted circle.

310

311 To study the membrane roughness before and after CNTs coating, AFM was used to  
 312 characterize the membrane surface topography[45]. The combination of CNTs's nanostructure  
 313 and nanofibrous microstructure can achieve a hierarchical structure as shown in Figure 1(e).  
 314 This unique structure is essential to enhance the roughness and achieve superwetting properties  
 315 accompanied by PVA crosslinking. In the underwater condition, this superhydrophilic  
 316 hierarchical structure is able to absorb water, form a water protective surface layer, provide  
 317 water pockets between oils and membrane surface, and thus leading to the lowest contact area  
 318 of applied droplet and resulting in the reduction of adhesive force to oil droplet[26]. It is shown  
 319 in **Figure 6** (b) that PAN and CNTs-PAN membranes have a significant higher roughness than  
 320 the commercial membrane developed by phase inversion technology. The 3D images of the

321 membrane surfaces show that the additional CNTs layer covers the voids between nanofibers  
 322 and results in the reduction of overall surface roughness in the scan range of  $5\ \mu\text{m} \times 5\ \mu\text{m}$ .  
 323 Interestingly, a pair of representative AFM line profiles in **Figure 6 (c)** shows that although  
 324 the overall surface roughness value of CNTs-PAN membrane is lower than that of the PAN  
 325 membrane, it (in green) has a higher peak density (2.6 peaks/ $\mu\text{m}$ ) than that of PAN membrane  
 326 (1.8 peaks/ $\mu\text{m}$ ), indicating its nano-roughness contributing to the hierarchical structure. The  
 327 peak density of line scan is of great importance for characterizing the roughness of nano  
 328 composite membrane as the membrane surface roughness is dependent on scan range and  
 329 location.  
 330



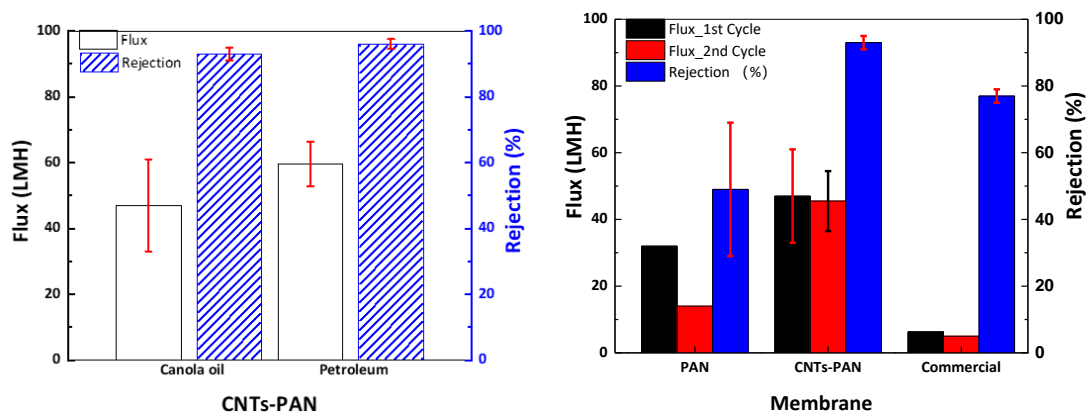
331 **Figure 6** (a) Schematic and wetting of the three different surfaces. The largest contact area  
 332 between the droplet and the surface is given in flat and microstructured surfaces and is  
 333 minimized in hierarchical structured surfaces. (b) 3-D surface topography and roughness of the  
 334 three membrane surfaces by AFM. (c) Surface height maps and corresponding line scan  
 335 profiles of PAN and CNTs-PAN membrane using an AFM. Height peaks were marked in red  
 336 (PAN) and green (CNTs-PAN) for calculating the peak density along the scanning length.  
 337

338

### 339 3.5 Oil removal from oil-in-water emulsions

340 As the key performance indexes of a separation membrane, the permeation flux and rejection  
341 of CNTs-PAN were assessed, and the results are shown in **Figure 7(a)**. The CNTs-PAN  
342 membrane allows continuous water phase to pass through and shows water fluxes of 48 LMH  
343 and 60 LMH at an applied pressure of 20 kPa for canola-in-water and petroleum-in-water  
344 emulsions, respectively. The water flux of the CNTs-PAN membrane is three times higher than  
345 our previously reported membrane when used to treat the same petroleum-in-water  
346 emulsions[21]. The CNTs-PAN membrane shows a rejection of 93% and 96% for canola-in-  
347 water and petroleum-in-water emulsions, respectively. **Table 2** summarizes the oil droplet size  
348 of emulsions. It can be seen that canola oil emulsion has the smallest oil droplet down to  
349  $1.46\pm 0.74\ \mu\text{m}$ , and  $2.78\pm 0.02\ \mu\text{m}$  for petroleum emulsion. The similar emulsion droplet sizes  
350 of the feed solutions before and after tests indicate that emulsions are stable during the tests.  
351 Therefore, the difference in permeate flux and rejection of the as-prepared membrane for  
352 different oil emulsions depends on the oil droplet size. The membrane shows lower flux in  
353 treating canola oil emulsions due to its relatively smaller oil droplets and higher viscosity, thus  
354 we used canola oil as the model solution for further study.

355

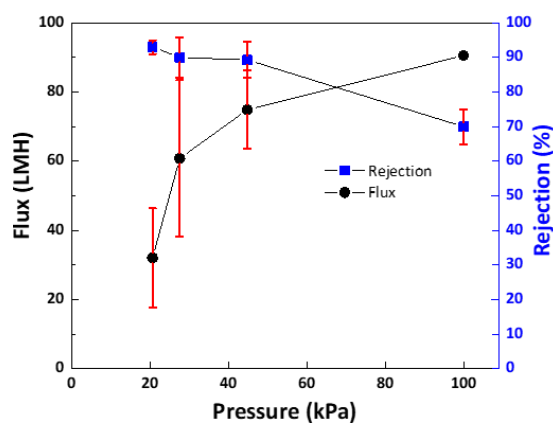


356

(a)

(b)

357



358

359

(c)

360 **Figure 7** (a) Permeate fluxes and rejections to various oil-in-water emulsions of membrane  
 361 CNTs-PAN. (b) Permeate fluxes and rejections of the three membranes, PAN, CNTs-PAN and  
 362 a commercial membrane with similar pore sizes. Feed emulsion compositions: 1000 ppm oil,  
 363 100 ppm surfactant; testing condition: 20 kPa applied pressure, 0.18 m/s surface velocity. (c)  
 364 Dependence of CNTs-PAN separation performance on working pressure.

365

366

**Table 2** Oil in water emulsion particle size characterized by Mastersizer

Feed	Feed <sup>(1)</sup>	Membrane	Feed, 1 hour <sup>(2)</sup>
	Mean droplet size		Mean droplet size
1000 ppm Petroleum, 100ppm Tween 20	2.78±0.02 μm	CNTs_PAN	3.53±0.12 μm
1000 ppm Canola oil, 100ppm Tween 20	1.46±0.74μm	CNTs_PAN	2.65 ±0.35 μm
1000 ppm Canola oil, 100ppm Tween 20	2.74 ±0. 1μm	Commercial	2.83 ±0.07 μm

367

368 Note: (1) Feed samples were collected before the filtration test and was kept for 1 hour before Masterizer  
 369 characterization. (2) Feed, 1hour: means the samples were collected after a 1-hour crossflow filtration  
 370 test and characterized by Mastersizer.

371

372 **Figure 7(b)** presents the water flux and rejection to canola oil of the as-prepared PAN, CNTs-  
 373 PAN membranes and a commercial membrane. The commercial membrane with a mean pore  
 374 size 0.3 μm shows a flux of 6.3 LMH and 77 ± 2% rejection at 20 kPa. **Due to the larger**  
 375 **membrane pores and capillary effects, the superhydrophilic nanofibrous membranes usually**  
 376 **exhibit better water permeability. The PAN and CNTs-PAN membranes exhibit excellent pure**  
 377 **water permeability of 420 ± 51 LMH and 157 ± 64 LMH at a testing pressure of 20 kPa,**  
 378 **respectively.** In the oil/water separation filtration, the nanofibrous membrane PAN exhibits a  
 379 comparatively lower flux, lower rejection and lower flux recovery rate due to its large open

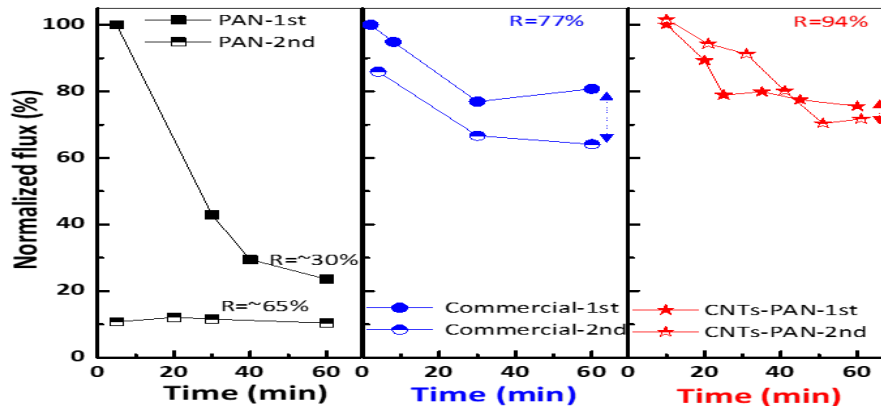
380 surface area, which was eventually fouled by the oil clogging. In contrast, the CNTs-PAN  
381 membrane shows a water flux up to  $47\pm 14$  LMH and  $93\pm 2\%$  rejection and a nearly 100%  
382 recovery rate in the second cycle without any cleaning. It is believed that the on-top formed  
383 additional ultrathin superhydrophilic hierarchical CNTs layer absorbed the water and formed a  
384 selective and protective layer to rapidly separate the oil droplets from water, protecting the  
385 membrane surface from oil and surfactant clogging, and thus guaranteeing an easy flux  
386 recovery. **Figure 7(c)** presents water flux and oil rejection as a function of applied hydraulic  
387 pressure of CNTs-PAN membrane. It can be seen that the current membrane can withstand a  
388 pressure up to 40 kPa, which indicates its mechanical robustness in the real application. The  
389 membrane shows a water flux of 70 LMH and 90% oil rejection at 40 kPa.

390

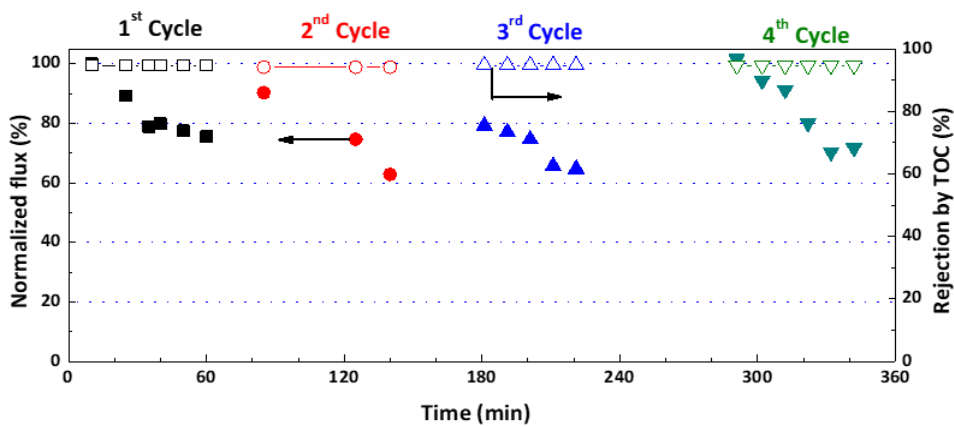
### 391 3.6 Self-cleaning behaviour

392 **Figure 8(a)** shows the normalized permeate fluxes and oil rejections of the PAN membrane,  
393 commercial membrane and CNTs-PAN membranes. It should be noted that no physical or  
394 chemical cleaning was conducted between the filtration cycles. The flux of the PAN decreases  
395 greatly in the first cycle and can only recover 10% of its initial flux in the second cycle. The  
396 flux of the commercial membrane decreases over time and loses its initial flux of 20% after the  
397 first cycle test and 35% after the second cycle test. The initial flux of the commercial membrane  
398 in the second cycle test is only recovered to 86 % after the 20 min rest. Compared with the  
399 commercial membrane, the CNTs-PAN membrane possesses nearly full recovery rates of its  
400 flux and oil rejection. Moreover, the CNTs-PAN membrane shows even higher separation  
401 efficiency of 94%, compared with the commercial membrane (77%). Membrane compaction  
402 [21] and oil fouling [7] should be responsible for the flux reduction during both tests. After  
403 resting the commercial membrane for 20 min, the declined flux due to membrane compaction  
404 could be recovered. Thus, the commercial membrane flux increased from 80% to 86% of its

405 initial flux. However, the flux reduction due to membrane fouling cannot be recovered. In  
 406 contrast, attributed to the anti-fouling and self-cleaning properties of the superhydrophilic  
 407 surface and the rebound of membrane compaction, the CNTs-PAN membrane's flux can be  
 408 fully recovered to its initial flux.  
 409

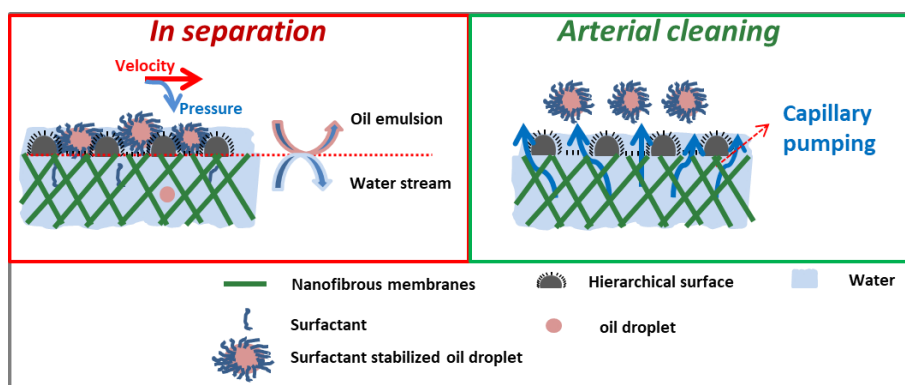


(a)



(b)

413  
 414



415

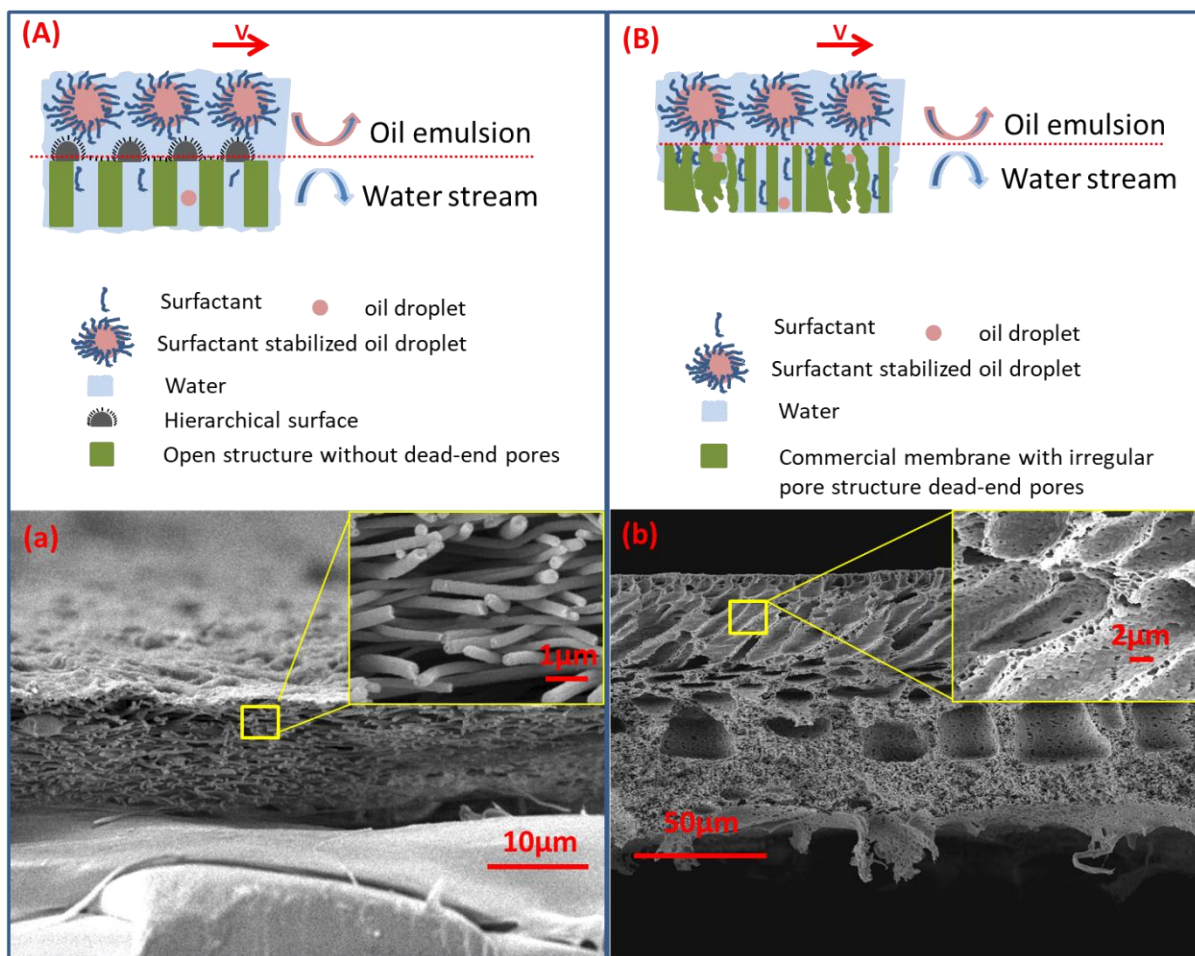
416

(c)

417 **Figure 8.** (a) Normalized permeate flux of a PAN (left), commercial membrane (middle) and  
 418 CNTs-PAN membrane (right) in a filtration cycle study. Feed emulsion: 1000 ppm canola oil,  
 419 100 ppm surfactant. No physical or chemical cleaning process was conducted between 1<sup>st</sup> and  
 420 2<sup>nd</sup> round test. (b) Long term study of the CNTs-PAN membrane in oil-in-water emulsion  
 421 separation in a filtration cycle study. Feed emulsion: Feed emulsion: 1000 ppm canola oil, 100  
 422 ppm surfactant. No physical or chemical cleaning process was conducted between round tests.  
 423 (c) Schematic of highly efficient flux recovery and self-cleaning based on capillary pumping  
 424 assisted with superhydrophilic surfaces and micro channels in CNTs-PAN membranes.

425

426 To further confirm this phenomenon, we evaluated the CNTs-PAN membrane in 4-cycle tests  
 427 as shown in **Figure 8 (b)**. The CNTs-PAN membrane shows a promising flux recovery in the  
 428 four cycles without cleaning. A hypothesis is proposed to explain this excellent flux recovery  
 429 ability. As illustrated in **Figure 8(c)**, after releasing the pressure applied on membrane surface,  
 430 the capillary effect in the enormous micro-channels of CNTs layer can draw the permeate water  
 431 from support layer and force the water up-flow. The up-flow permeate water is able to purge  
 432 out the surfactant and oil droplets trapped in membrane pores and clean the membrane, which  
 433 should prolong the membrane lifespan. On the contrary, the surfactant and oil droplets trapped  
 434 in the membrane with irregular pore structure, high tortuosity and dead-end pore structure, are  
 435 hard to be cleaned by backwash and consequently contaminate the membrane irreversibly.  
 436 **Figure 9** presents the schematical drawing to illustrate the possible mechanisms. The video  
 437 (video 2) presented in the support information (SI) demonstrates that membrane surface  
 438 remains its underwater superoleophobic property well after the long-term filtration test.

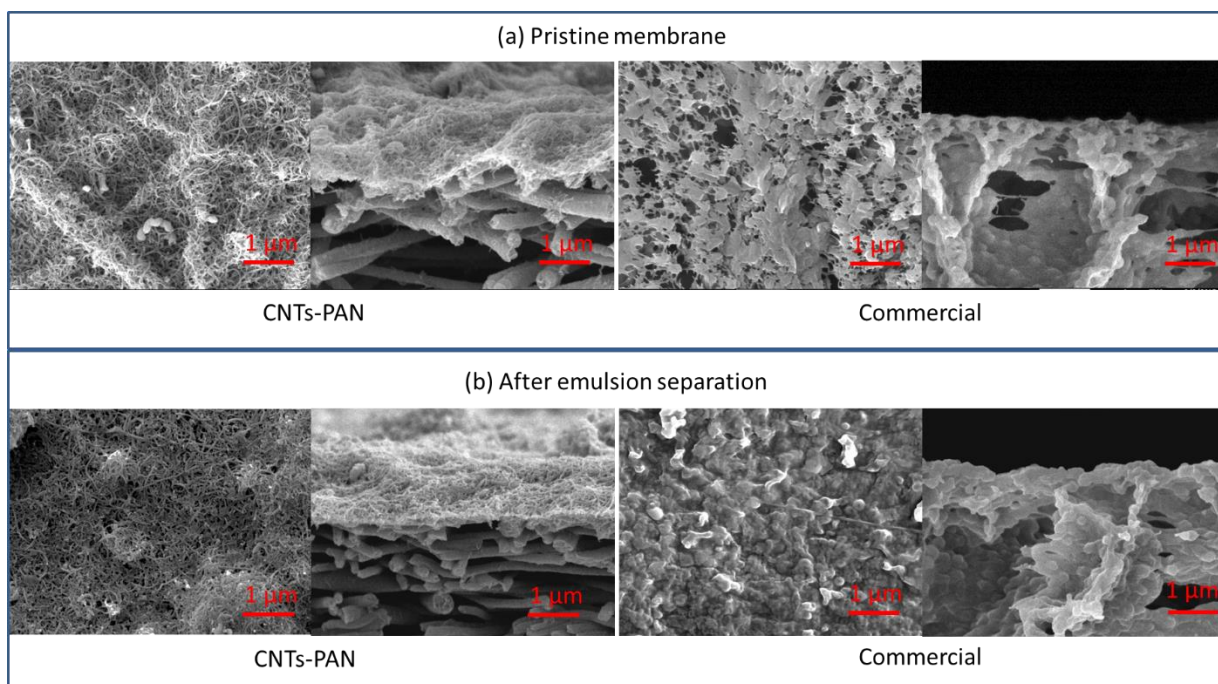


439

440 **Figure 9** schematically drawing of the surfactant-stabilized oil droplet interaction with (A)  
 441 CNTs-PAN and (B) commercial membrane with irregular pore structure. The corresponding  
 442 bottom FESEM group images illustrate the aforesaid (a) open and connected pore structures  
 443 and (b) irregular pore.

444

445 To further demonstrate the self-cleaning properties of CNTs-PAN membrane during oil/water  
 446 separation process, the surface and cross-sectional FESEM images before and after the 4-hour  
 447 cross-flow filtration operation are presented in **Figure 10**. The used CNTs-PAN membrane  
 448 still exhibited a clean micro/nano-structured surface as before, while the commercial  
 449 membrane was contaminated with the surfactants and oils.



450

451 **Figure 10** FESEM images of CNTs-PAN hierarchical membrane and the commercial  
 452 microfiltration membrane (a) before and (b) after the filtration tests.

453

454 The as-prepared ultra-thin superhydrophilic CNTs layer can absorb water as a selective layer  
 455 to remove oil droplets from surfactant-stabilized oil-in-water emulsions, and the function layer  
 456 can protect the support from contamination by surfactant and oil droplets. Moreover, the highly  
 457 porous and interconnected CNTs rejection layer and the nanofibrous layer consist of open and  
 458 active channels for penetrated oil droplet and surfactants, which promise its self-cleaning  
 459 property by the continuously up-flowed permeate water. In contrast, the dead-end pores of the  
 460 membranes prepared by conventional phase-inversion method may be blocked by the passed  
 461 surfactants, which can alter membrane original wettability and reduce membrane selectivity  
 462 and permeability.

463

#### 464 **4. Conclusions**

465 A novel TFNC membrane was successfully developed by spraying and crosslinking an  
 466 ultrathin superhydrophilic CNTs selective layer on the PAN nanofiber matrix. The as-prepared

467 ultra-thin superhydrophilic CNTs layer can absorb water as a selective layer to remove oil  
468 droplets from surfactant-stabilized oil-in-water emulsions, attributed to its in-air  
469 superhydrophilic and underwater superoleophobic surface. Meanwhile, the function layer can  
470 protect the support from contamination by surfactant and oil droplets. Moreover, the highly  
471 porous and interconnected CNTs rejection layer and the nanofibrous layer consist of open and  
472 active channels for penetrated oil droplet and surfactants, which promise its self-cleaning  
473 property by the continuously up-flowed permeate water. In contrast, the dead-end pores of the  
474 membranes prepared by conventional phase-inversion method may be blocked by the passed  
475 surfactants, which can alter membrane original wettability and reduce membrane selectivity  
476 and permeability. This work provides a new insight for design and development of membranes  
477 for oil-in-water emulsion separation and other similar separation processes which suffer from  
478 membrane fouling and clogging.

479

## 480 **5. Conflicts of interest**

481 There are no conflicts to declare

482

## 483 **6. Acknowledgements**

484 We acknowledge funding support from Singapore Economic Development Board to the  
485 Singapore Membrane Technology Centre (SMTC).

486

## 487 **SUPPORTING INFORMATION**

488 Two demonstrative videos are presented in the support information for a better view of the  
489 under superoleophobic. Two videos, Video 1 and Video 2, before and after filtration long-term  
490 test demonstrate that membrane surface preserve its underwater superoleophobic well after the

491 long-term filtration test. This material is available free of charge via the Internet at  
492 <http://pubs.acs.org>.

### 493 **References:**

#### 494 **Uncategorized References**

- 495 [1] N.L. Fahrenfeld, H. Delos Reyes, A. Eramo, D.M. Akob, A.C. Mumford, I.M. Cozzarelli, Shifts in  
496 microbial community structure and function in surface waters impacted by unconventional oil and  
497 gas wastewater revealed by metagenomics, *Science of The Total Environment*, 580 (2017) 1205-  
498 1213.
- 499 [2] I.M. Cozzarelli, K.J. Skalak, D.B. Kent, M.A. Engle, A. Benthem, A.C. Mumford, K. Haase, A. Farag,  
500 D. Harper, S.C. Nagel, L.R. Iwanowicz, W.H. Orem, D.M. Akob, J.B. Jaeschke, J. Galloway, M. Kohler,  
501 D.L. Stoliker, G.D. Jolly, Environmental signatures and effects of an oil and gas wastewater spill in the  
502 Williston Basin, North Dakota, *Science of The Total Environment*, 579 (2017) 1781-1793.
- 503 [3] C.H. Peterson, S.D. Rice, J.W. Short, D. Esler, J.L. Bodkin, B.E. Ballachey, D.B. Irons, Long-Term  
504 Ecosystem Response to the Exxon Valdez Oil Spill, *Science*, 302 (2003) 2082-2086.
- 505 [4] T. Sirivedhin, L. Dallbauman, Organic matrix in produced water from the Osage-Skiatook  
506 Petroleum Environmental Research site, Osage county, Oklahoma, *Chemosphere*, 57 (2004) 463-469.
- 507 [5] Y. Peng, Z. Guo, Recent advances in biomimetic thin membranes applied in emulsified oil/water  
508 separation, *Journal of Materials Chemistry A*, 4 (2016) 15749-15770.
- 509 [6] Z. Chu, Y. Feng, S. Seeger, Oil/Water Separation with Selective Superantwetting/Superwetting  
510 Surface Materials, *Angewandte Chemie International Edition*, 54 (2015) 2328-2338.
- 511 [7] B. Chakrabarty, A.K. Ghoshal, M.K. Purkait, Ultrafiltration of stable oil-in-water emulsion by  
512 polysulfone membrane, *Journal of Membrane Science*, 325 (2008) 427-437.
- 513 [8] S. Maphutha, K. Moothi, M. Meyyappan, S.E. Iyuke, A carbon nanotube-infused polysulfone  
514 membrane with polyvinyl alcohol layer for treating oil-containing waste water, *Sci Rep*, 3 (2013)  
515 1509.
- 516 [9] B. Chakrabarty, A.K. Ghoshal, M.K. Purkait, Cross-flow ultrafiltration of stable oil-in-water  
517 emulsion using polysulfone membranes, *Chem Eng J*, 165 (2010) 447-456.
- 518 [10] X. Zhu, A. Dudchenko, X. Gu, D. Jassby, Surfactant-stabilized oil separation from water using  
519 ultrafiltration and nanofiltration, *Journal of Membrane Science*, 529 (2017) 159-169.
- 520 [11] L. Yu, M. Han, F. He, A review of treating oily wastewater, *Arabian Journal of Chemistry*, 10  
521 (2017) S1913-S1922.
- 522 [12] Y. Wang, X. Gong, Special oleophobic and hydrophilic surfaces: approaches, mechanisms, and  
523 applications, *Journal of Materials Chemistry A*, 5 (2017) 3759-3773.
- 524 [13] S. Wang, K. Liu, X. Yao, L. Jiang, Bioinspired Surfaces with Superwettability: New Insight on  
525 Theory, Design, and Applications, *Chemical Reviews*, 115 (2015) 8230-8293.
- 526 [14] Z. Shi, W. Zhang, F. Zhang, X. Liu, D. Wang, J. Jin, L. Jiang, Ultrafast Separation of Emulsified  
527 Oil/Water Mixtures by Ultrathin Free-Standing Single-Walled Carbon Nanotube Network Films,  
528 *Advanced Materials*, 25 (2013) 2422-2427.
- 529 [15] M.H. Tai, P. Gao, B.Y.L. Tan, D.D. Sun, J.O. Leckie, Highly Efficient and Flexible Electrospun  
530 Carbon-Silica Nanofibrous Membrane for Ultrafast Gravity-Driven Oil-Water Separation, *ACS*  
531 *Applied Materials & Interfaces*, 6 (2014) 9393-9401.
- 532 [16] S. Zhang, G. Jiang, S. Gao, H. Jin, Y. Zhu, F. Zhang, J. Jin, Cupric Phosphate Nanosheets-Wrapped  
533 Inorganic Membranes with Superhydrophilic and Outstanding Anticrude Oil-Fouling Property for  
534 Oil/Water Separation, *ACS Nano*, 12 (2018) 795-803.
- 535 [17] W. Zhang, Y. Zhu, X. Liu, D. Wang, J. Li, L. Jiang, J. Jin, Salt - induced fabrication of  
536 superhydrophilic and underwater superoleophobic PAA - g - PVDF membranes for effective  
537 separation of oil-in-water emulsions, *Angewandte Chemie International Edition*, 53 (2014) 856-860.

538 [18] P.-C. Chen, Z.-K. Xu, Mineral-coated polymer membranes with superhydrophilicity and  
539 underwater superoleophobicity for effective oil/water separation, *Scientific reports*, 3 (2013) 2776.

540 [19] F. Zhang, W.B. Zhang, Z. Shi, D. Wang, J. Jin, L. Jiang, Nanowire-Haired Inorganic Membranes  
541 with Superhydrophilicity and Underwater Ultralow Adhesive Superoleophobicity for High-Efficiency  
542 Oil/Water Separation, *Advanced Materials*, 25 (2013) 4192-4198.

543 [20] Y. Liao, C.-H. Loh, M. Tian, R. Wang, A.G. Fane, Progress in electrospun polymeric nanofibrous  
544 membranes for water treatment: Fabrication, modification and applications, *Progress in Polymer  
545 Science*, 77 (2018) 69-94.

546 [21] Y. Liao, M. Tian, R. Wang, A high-performance and robust membrane with switchable super-  
547 wettability for oil/water separation under ultralow pressure, *Journal of Membrane Science*, 543  
548 (2017) 123-132.

549 [22] G.-d. Kang, Y.-m. Cao, Development of antifouling reverse osmosis membranes for water  
550 treatment: a review, *Water research*, 46 (2012) 584-600.

551 [23] P. Ragesh, V.A. Ganesh, S.V. Nair, A.S. Nair, A review on 'self-cleaning and multifunctional  
552 materials', *Journal of Materials chemistry A*, 2 (2014) 14773-14797.

553 [24] C.H. Lee, N. Johnson, J. Drelich, Y.K. Yap, The performance of superhydrophobic and  
554 superoleophilic carbon nanotube meshes in water-oil filtration, *Carbon*, 49 (2011) 669-676.

555 [25] H. Gao, Y. Yang, O. Akampumuza, J. Hou, H. Zhang, X. Qin, A low filtration resistance three-  
556 dimensional composite membrane fabricated via free surface electrospinning for effective PM2.5  
557 capture, *Environmental Science: Nano*, 4 (2017) 864-875.

558 [26] Y.C. Jung, B. Bhushan, Mechanically durable carbon nanotube- composite hierarchical  
559 structures with superhydrophobicity, self-cleaning, and low-drag, *ACS nano*, 3 (2009) 4155-4163.

560 [27] W. Qing, X. Shi, Y. Deng, W. Zhang, J. Wang, C.Y. Tang, Robust superhydrophobic-superoleophilic  
561 polytetrafluoroethylene nanofibrous membrane for oil/water separation, *Journal of Membrane  
562 Science*, 540 (2017) 354-361.

563 [28] L. Eskandarian, E. Pajootan, M. Arami, Novel Super Adsorbent Molecules, Carbon Nanotubes  
564 Modified by Dendrimer Miniature Structure, for the Removal of Trace Organic Dyes, *Industrial &  
565 Engineering Chemistry Research*, 53 (2014) 14841-14853.

566 [29] M. Muoth, T. Helbling, L. Durrer, S.W. Lee, C. Roman, C. Hierold, Hysteresis-free operation of  
567 suspended carbon nanotube transistors, *Nat Nanotechnol*, 5 (2010) 589-592.

568 [30] K. Goh, L. Setiawan, L. Wei, W. Jiang, R. Wang, Y. Chen, Fabrication of novel functionalized  
569 multi-walled carbon nanotube immobilized hollow fiber membranes for enhanced performance in  
570 forward osmosis process, *Journal of membrane science*, 446 (2013) 244-254.

571 [31] A.V. Dudchenko, J. Rolf, K. Russell, W. Duan, D. Jassby, Organic fouling inhibition on electrically  
572 conducting carbon nanotube-polyvinyl alcohol composite ultrafiltration membranes, *Journal of  
573 Membrane Science*, 468 (2014) 1-10.

574 [32] J. Farahbaksh, M. Delnavaz, V. Vatanpour, Investigation of raw and oxidized multiwalled carbon  
575 nanotubes in fabrication of reverse osmosis polyamide membranes for improvement in desalination  
576 and antifouling properties, *Desalination*, 410 (2017) 1-9.

577 [33] X. Wang, X. Chen, K. Yoon, D. Fang, B.S. Hsiao, B. Chu, High flux filtration medium based on  
578 nanofibrous substrate with hydrophilic nanocomposite coating, *Environmental science &  
579 technology*, 39 (2005) 7684-7691.

580 [34] S. Qiu, L. Wu, X. Pan, L. Zhang, H. Chen, C. Gao, Preparation and properties of functionalized  
581 carbon nanotube/PSF blend ultrafiltration membranes, *Journal of Membrane Science*, 342 (2009)  
582 165-172.

583 [35] M.A. Shannon, P.W. Bohn, M. Elimelech, J.G. Georgiadis, B.J. Marinas, A.M. Mayes, Science and  
584 technology for water purification in the coming decades, *Nature*, 452 (2008) 301-310.

585 [36] M. Whitby, N. Quirke, Fluid flow in carbon nanotubes and nanopipes, *Nature Nanotechnology*, 2  
586 (2007) 87-94.

587 [37] W. Guo, J. Hansson, W. van der Wijngaart, Capillary pumping independent of the liquid surface  
588 energy and viscosity, *Microsystems & Nanoengineering*, 4 (2018) 2.

589 [38] Y. Liao, R. Wang, M. Tian, C. Qiu, A.G. Fane, Fabrication of polyvinylidene fluoride (PVDF)  
590 nanofiber membranes by electro-spinning for direct contact membrane distillation, *Journal of*  
591 *Membrane Science*, 425 (2013) 30-39.

592 [39] M. Tian, C. Qiu, Y. Liao, S.R. Chou, R. Wang, Preparation of polyamide thin film composite  
593 forward osmosis membranes using electrospun polyvinylidene fluoride (PVDF) nanofibers as  
594 substrates, 118 (2013) 727-736.

595 [40] B. Bolto, T. Tran, M. Hoang, Z. Xie, Crosslinked poly(vinyl alcohol) membranes, *Progress in*  
596 *Polymer Science*, 34 (2009) 969-981.

597 [41] M. Tian, R. Wang, K. Goh, Y. Liao, A.G. Fane, Synthesis and characterization of high-performance  
598 novel thin film nanocomposite PRO membranes with tiered nanofiber support reinforced by  
599 functionalized carbon nanotubes, *Journal of Membrane Science*, 486 (2015) 151-160.

600 [42] R. Rudra, V. Kumar, P.P. Kundu, Acid catalysed cross-linking of poly vinyl alcohol (PVA) by  
601 glutaraldehyde: effect of crosslink density on the characteristics of PVA membranes used in single  
602 chambered microbial fuel cells, *Rsc Adv*, 5 (2015) 83436-83447.

603 [43] J. Ge, J. Zhang, F. Wang, Z. Li, J. Yu, B. Ding, Superhydrophilic and underwater superoleophobic  
604 nanofibrous membrane with hierarchical structured skin for effective oil-in-water emulsion  
605 separation, *Journal of Materials Chemistry A*, 5 (2017) 497-502.

606 [44] J. Gohil, P. Ray, Polyvinyl alcohol as the barrier layer in thin film composite nanofiltration  
607 membranes: Preparation, characterization, and performance evaluation, *Journal of colloid and*  
608 *interface science*, 338 (2009) 121-127.

609 [45] Y. Huang, H. Li, L. Wang, Y. Qiao, C. Tang, C. Jung, Y. Yoon, S. Li, M. Yu, Ultrafiltration  
610 Membranes with Structure-Optimized Graphene-Oxide Coatings for Antifouling Oil/Water  
611 Separation, *Advanced Materials Interfaces*, 2 (2015) 1400433.

612